Article

Bi^{3+} and Eu^{3+} Activated Luminescent Behaviors in Non-Stoichiometric LaO$_{0.65}$F$_{1.7}$ Structure

Sungjun Yang and Sangmoon Park *

Division of Energy Convergence Engineering, Major in Energy & Applied Chemistry, Silla University, Busan 46958, Korea; qse7417@naver.com
* Correspondence: spark@silla.ac.kr; Tel.: +82-51-999-5891

Abstract: Optical materials composed of La$_{1-p-q}$Bi$_p$Eu$_q$O$_{0.65}$F$_{1.7}$ (p = 0.001–0.05, q = 0–0.1) were prepared via a solid-state reaction using La(Bi,Eu)$_2$O$_3$ and NH$_4$F precursors at 1050 °C for two hours. X-ray diffraction patterns of the phosphors were obtained permitting the calculation of unit-cell parameters. The two La^{3+} cation sites were clearly distinguished by exploiting the photoluminescence excitation and emission spectra through Bi^{3+} and Eu^{3+} transitions in the non-stoichiometric host lattice. Energy transfer from Bi^{3+} to Eu^{3+} upon excitation with 286 nm radiation and its mechanism in the Bi^{3+}- and Eu^{3+}-doped host structures is discussed. The desired Commission Internationale de l'Eclairage values, including emissions in blue-green, white, and red wavelength regions, were obtained from the Bi^{3+}- and Eu^{3+}-doped LaO$_{0.65}$F$_{1.7}$ phosphors.

Keywords: X-ray diffraction; phosphors; Bi^{3+}, Eu^{3+} transitions; energy transfer

1. Introduction

Ce^{3+}-doped Y$_3$Al$_5$O$_{12}$ (YAG) yellow phosphors are commonly used with blue light-emitting diodes (LEDs) to create white light sources [1–5]. The Ce^{3+} ions emit in the blue to yellow wavelength regions assigned by 5d^1 to 4f^1 transitions when excited by ultraviolet (UV) to visible radiation in various host lattices [6–9]. The Ce^{3+} ion, as a donor, enables efficient energy transfer, improving the emission from acceptors, such as Tb^{3+} or Mn^{2+} ions in the host structures [10–18]. The Bi^{3+} ion is an active luminescent center emitting blue to green light assigned to 6$s^1$6p^1 to 6s^2 transitions when excited by UV to near UV wavelength regions in host lattices [19–21]. The energy levels of the Bi^{3+} 6s^2–6$s^1$6p^1 transitions consist of ^{1}S$_0$ and the triplet ^{3}P$_J$ (J = 0, 1, or 2) and singlet ^{1}P$_1$ states. The ^{1}S$_0$ to ^{3}P$_1$, ^{1}P$_1$ transitions occur via spin-orbital coupling [19–21]. The states of the ^{1}S$_0$ to ^{3}P$_0$ and ^{3}P$_2$ transitions are forbidden [19–21]. Like Ce^{3+} ions, Bi^{3+} ions act as sensitizers to enhance the anticipated emission light from acceptors, such as Eu^{3+} or Tb^{3+} ions in host structures, by facilitating efficient energy transfer [22–26].

The up-conversion properties of Er^{3+}- and Yb^{3+}-doped LaO$_{0.65}$F$_{1.7}$ compounds were exploited under 980 nm diode laser excitation in a previous study [27]. This non-stoichiometric LaO$_{0.65}$F$_{1.7}$ host comprises alternating stacked LaO$_2$F$_7$ and LaO$_3$F$_7$ layers along the c axis with tetragonal space group *P4/nmm*, as shown in Figure 1 [27,28]. The 9- and 10-coordinated La^{3+} sites in the LaF(1)$_3$F(2)$_2$O$_2$F(3)$_2$ and LaF(1)$_4$F(2)O$_3$F(3)$_2$ polyhedrons are located in accordance with the La(F(1)$_{0.86}$V$_{0.14}$)(F(2)$_{0.35}$O$_{0.65}$)(F(3)$_{0.49}$) lattice of the LaO$_{0.65}$F$_{1.7}$ host structure [27,28]. Notably, the nine-fold LaF(1)$_3$VF(2)$_2$O$_2$F(3)$_2$ polyhedron contains a vacancy (V) associated with the F(1) anion.

In this study, Bi^{3+} and Eu^{3+} were substituted into LaO$_{0.65}$F$_{1.7}$ compounds that were synthesized by a solid-state method using NH$_4$F flux in air. The unit-cell parameters of the phosphors were calculated. The excitation and emission luminescence spectra of the La$_{1-p-q}$Bi$_p$Eu$_q$O$_{0.65}$F$_{1.7}$ (p = 0.001–0.05, q = 0–0.1) phosphors were investigated with respect to the site dependency of Bi^{3+} and Eu^{3+} ions in the host

structure. The energy transfer mechanism from Bi^{3+} to Eu^{3+} in the phosphors was explored. Commission Internationale de l'Eclairage (CIE) chromaticity coordinates of the phosphors were obtained.
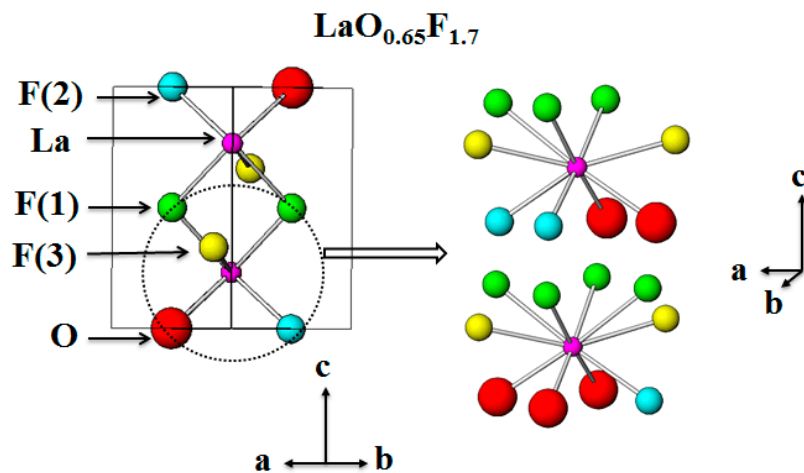
Figure 1. The structure of tetragonal $LaO_{0.65}F_{1.7}$ host lattice.

2. Materials and Methods

Phosphors of $La_{1-p-q}Bi_pEu_qO_{0.65}F_{1.7}$ (p = 0.005–0.05, q = 0–0.1) were prepared by heating the appropriate amounts of La_2O_3 (Alfa 99.9%), Bi_2O_3 (Alfa 99.99%), Eu_2O_3 (Alfa 99.9%), and NH_4F (Alfa 99%). Powdered samples with 1:2 molar ratios of $La(Bi,Eu)O_{3/2}$ and NH_4F were used to prepare nonstoichiometric $LaO_{0.65}F_{1.7}$:Bi^{3+}, Eu^{3+}. The precursors were mixed with an agate mortar and pestle and subsequently heated at 1050 °C for 2 h in air [27]. The La_2O_3 precursor was pre-heated at 700 °C for 3 h to remove hydroxide in the sample. Phase identification of the phosphors was performed using a Shimadzu XRD-6000 powder diffractometer (Cu-Kα radiation, Shimadzu CO., Kyoto, Japan). The Rietveld refinement program Rietica was used for the unit-cell parameter calculations. UV spectroscopy of the excitation and emission spectra of the phosphors was measured using spectrofluorometers (Sinco Fluoromate FS-2, Sinco CO., Seoul, Korea).

3. Results and Discussion

The crystallographic phase of the $La_{1-p-q}Bi_pEu_qO_{0.65}F_{1.7}$ (p = 0.001–0.05, q = 0–0.1) powders was identified using powder X-ray diffraction (XRD) patterns. The calculated XRD pattern of the tetragonal $LaO_{0.65}F_{1.7}$ (ICSD 40371) structure is shown in Figure 2A. Figure 2B–F show the XRD patterns of non-stoichiometric $La_{1-p-q}Bi_pEu_qO_{0.65}F_{1.7}$ phosphors (p = 0.01 and q = 0, p = 0.05 and q = 0, p = 0 and q = 0.05, p = 0 and q = 0.1, and p = 0.01 and q = 0.1, respectively), synthesized by the mixing of $\frac{1}{2}La(Bi,Eu)_2O_3$ and NH_4F at 1050 °C in air. The XRD patterns of the obtained phosphors in Figure 2B–F show a single-phase structure without any noticeable impurities indexed to a tetragonal unit cell. The unit cells of $La_{0.99}Bi_{0.01}O_{0.65}F_{1.7}$, $La_{0.95}Bi_{0.05}O_{0.65}F_{1.7}$, $La_{0.95}Eu_{0.05}O_{0.65}F_{1.7}$, $La_{0.9}Eu_{0.1}O_{0.65}F_{1.7}$, and $La_{0.89}Bi_{0.01}Eu_{0.1}O_{0.65}F_{1.7}$ phosphors were calculated to be a = 4.0934 (1) Å and c = 5.8336 (2) Å, a = 4.1018 (2) Å and c = 5.8315 (2) Å, a = 4.0833 (2) Å and c = 5.8162 (4) Å, a = 4.0788 (3) Å and c = 5.8095 (5) Å, and a = 4.0993(3) Å and c = 5.7712(6) Å, respectively, using the Rietveld refinement. The unit-cell parameters, including the cell volumes of the phosphors, are summarized in Table 1. The Bi^{3+} and Eu^{3+} ions, under these conditions, occupy 9- and 10-coordinated La^{3+} sites ($LaF(1)_3F(2)_2O_2F(3)_2$ and $LaF(1)_4F(2)O_3F(3)_2$) in the non-stoichiometric $LaO_{0.65}F_{1.7}$ structure, as shown in Figure 1 [27,28]. The single La^{3+} site comprises 56% 9-fold and 44% 10-fold polyhedrons in the $LaO_{0.65}F_{1.7}$ lattice based on the $La(F(1)_{0.86}V_{0.14})(F(2)_{0.35}O_{0.65})(F(3)_{0.49})$ formula. The 9- and 10- coordinated LaO_2F_7 and LaO_3F_7 polyhedrons in the non-stoichiometric unit cell are arrayed along the c-axis, as shown in Figure 1. When Bi^{3+} ions (r = 1.17 Å for 8 coordination number (CN)) were substituted for La^{3+} ions (r = 1.16 Å for 8 CN) in the $LaO_{0.65}F_{1.7}$ host lattice, gradual shifts in the positions of the various Bragg reflections

to lower angles with unit-cell expansion were observed, as shown in Figure 2B,C. When Eu^{3+} ions ($r = 1.066$ Å for 8 CN) were substituted for La^{3+} ions in the host lattice, gradual shifts in the positions of the various Bragg reflections to higher angles with unit-cell contraction were observed, as shown in Figure 2D,E. When the Bi^{3+} ions were doped in the $La_{0.9}Eu_{0.1}O_{0.65}F_{1.7}$ phosphors, no further shift to higher angles was observed in the $La_{0.89}Bi_{0.01}Eu_{0.1}O_{0.65}F_{1.7}$ phosphors, as shown in Figure 2F.
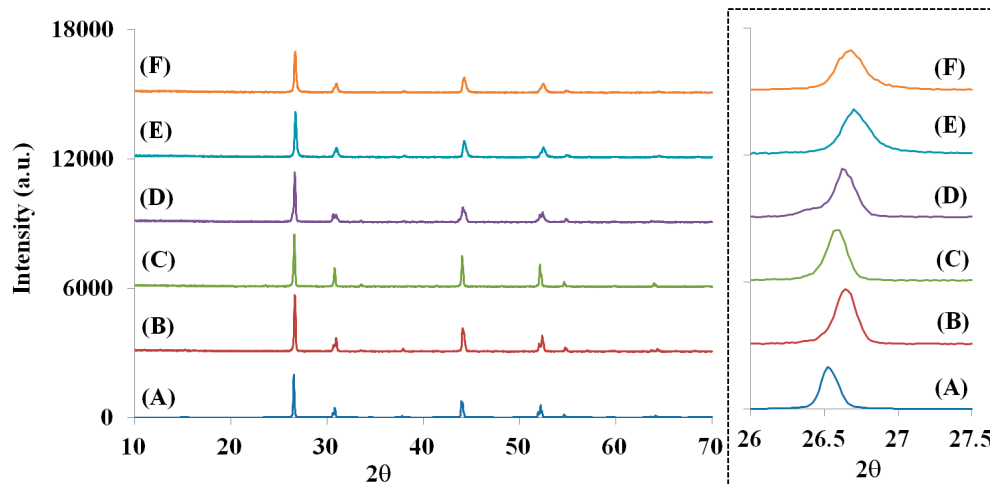
Figure 2. The calculated XRD patterns of (A) $LaO_{0.65}F_{1.7}$ (ICSD 40371) and the obtained XRD patterns of $La_{1-p-q}Bi_pEu_qO_{0.65}F_{1.7}$ phosphors (B) $p = 0.01$ and $q = 0$, (C) $p = 0.05$ and $q = 0$, (D) $p = 0$ and $q = 0.05$, (E) $p = 0$ and $q = 0.1$, and (F) $p = 0.01$ and $q = 0.1$.

Table 1. The unit-cell parameters with the cell volumes of the $La_{0.99}Bi_{0.01}O_{0.65}F_{1.7}$, $La_{0.95}Bi_{0.05}O_{0.65}F_{1.7}$, $La_{0.95}Eu_{0.05}O_{0.65}F_{1.7}$, $La_{0.9}Eu_{0.1}O_{0.65}F_{1.7}$, and $La_{0.89}Bi_{0.01}Eu_{0.1}O_{0.65}F_{1.7}$ phosphors.

Phosphors	a (Å)	c (Å)	V (Å^3)	R_p
$La_{0.99}Bi_{0.01}O_{0.65}F_{1.7}$	4.0934 (1)	5.8336 (2)	97.75 (1)	9.11
$La_{0.95}Bi_{0.05}O_{0.65}F_{1.7}$	4.1018 (2)	5.8315 (2)	98.11 (1)	9.98
$La_{0.95}Eu_{0.05}O_{0.65}F_{1.7}$	4.0833 (2)	5.8162 (4)	96.98 (1)	9.46
$La_{0.9}Eu_{0.1}O_{0.65}F_{1.7}$	4.0788 (3)	5.8095 (5)	96.65 (1)	8.95
$La_{0.89}Bi_{0.01}Eu_{0.1}O_{0.65}F_{1.7}$	4.0993 (3)	5.7712 (6)	96.98 (1)	9.62

　　Figure 3aA–E show the photoluminescence (PL), excitation (EX), and emission (EM) spectra of the Bi-doped $La_{1-p}Bi_pO_{0.65}F_{1.7}$ phosphors ($p = 0.001, 0.005, 0.01, 0.025,$ and 0.05, respectively). The excitation band centered near 278 and 286 nm in the $La_{0.99}Bi_{0.01}O_{0.65}F_{1.7}$ PL spectra is attributed to the $^1S_0 \rightarrow {}^3P_1$ transition of Bi^{3+} ions because the $^1S_0 \rightarrow {}^3P_0$ and $^1S_0 \rightarrow {}^3P_2$ transitions are forbidden from ground $^1S_0$ [19–26]. The blue emission spectra of the $LaO_{0.65}F_{1.7}$:Bi^{3+} phosphors revealed a broadband range from 350 to 650 nm, centered at approximately 497 nm, which is attributed to the intense $^3P_1 \rightarrow {}^1S_0$ transitions of the Bi^{3+} ions, as shown in Figure 3a. When the Bi^{3+} concentration in the host lattice was 1 mol %, the maximum emission intensity of the obtained phosphors was observed at the excitation wavelength of 278 nm, as shown in Figure 3aC. After the Bi^{3+} concentration was increased 2.5 mol % in the phosphors, the centered excitation peak shifted to a higher wavelength region from 278 to 286 nm, as shown in Figure 3aD,E. Thus, as the Bi^{3+} content in the $LaO_{0.65}F_{1.7}$ host lattice was increased and the excitation center of the $^1S_0 \rightarrow {}^3P_1$ transition of Bi^{3+} ions underwent a shift to a longer wavelength. The La^{3+} ion is coordinated by seven F^- and two O^{2-} anions ($LaF(1)_3F(2)_2O_2F(3)_2$), or seven F^- and three O^{2-} anions ($LaF(1)_4F(2)O_3F(3)_2$) in the $LaO_{0.65}F_{1.7}$ host structure [27,28]. As depicted in Figure 1, there was a vacancy associated with the F(1) anion in the $LaF(1)_3F(2)_2O_2F(3)_2$ polyhedron. Based on the ratios of oxygen and fluoride to lanthanum, the $LaF(1)_3F(2)_2O_2F(3)_2$ polyhedron had a lower oxygen ion covalency than $LaF(1)_4F(2)O_3F(3)_2$ polyhedrons in the structure. This observation indicated that Bi^{3+} ions are preferentially substituted in the nine-fold La site and subsequently doped into the

10-fold La site in the host structure. Figure 3b shows the excitation and emission PL spectra of the $La_{0.95}Eu_{0.05}O_{0.65}F_{1.7}$ phosphors. The charge-transfer bands (CTBs) and the *f–f* transitions of the Eu^{3+} activator in the host lattice were observed at 220–350 and 350–540 nm, respectively. Two CTBs centered at 290 and 320 nm were found in the excitation spectra because there were two La^{3+} sites associated with the $LaF(1)_3F(2)_2O_2F(3)_2$ and $LaF(1)_4F(2)O_3F(3)_2$ polyhedrons in the host structure. When Eu^{3+} ions were doped in the nine-coordinated La^{3+} site of the $LaF(1)_3F(2)_2O_2F(3)_2$ polyhedron, the center of the Eu^{3+} CTB transitions occurred at 290 nm. Additional energy was required to excite an electron from the Eu^{3+} ions in seven F^- and two O^{2-} containing lattices, compared to seven F^- and three O^{2-} polyhedrons.

The Eu^{3+} transitions of the emission spectra in the $La_{0.95}Eu_{0.05}O_{0.65}F_{1.7}$ phosphors exhibited both the $^5D_0-^7F_1$ magnetic dipole and the $^5D_0-^7F_2$ electric-dipole transitions, centered at 592 and 610 nm, respectively [29,30]. When the Eu^{3+} ions were substituted in no inversion site of the nine-coordinated polyhedron in the host lattice, the $^5D_0-^7F_2$ transition dominates. When the Eu^{3+} activators were doped into symmetric inversion site of the 10-fold polyhedron, the $^5D_0-^7F_1$ transition dominates. Figure 3c shows the excitation spectra of the $La_{0.95}Eu_{0.05}O_{0.65}F_{1.7}$ ($EX_{EM=610nm}$ and $EX_{EM=592nm}$) and the emission spectrum of $La_{0.99}Bi_{0.01}O_{0.65}F_{1.7}$ ($EM_{EX=286nm}$) phosphors. The efficiency of energy transfer from Bi^{3+} to Eu^{3+} was estimated by the spectral overlap between the excitation of the Eu^{3+} transition and the emission band of Bi^{3+} ions in the host lattice [31]. The excitation spectrum of the $La_{0.95}Eu_{0.05}O_{0.65}F_{1.7}$ ($EX_{EM=610nm}$) phosphor and the emission spectrum of the $La_{0.99}Bi_{0.01}O_{0.65}F_{1.7}$ ($EM_{EX=286nm}$) phosphor exhibited considerable overlap, as shown in the top of Figure 3c. This indicated that effective energy transfer from Bi^{3+} to Eu^{3+} ions occurs in the nine-coordinated La^{3+} site of the $LaF(1)_3F(2)_2O_2F(3)_2$ polyhedron in the $LaO_{0.65}F_{1.7}$ host structure. The individual transitions of Bi^{3+} and Eu^{3+} ions with the energy transfer from Bi^{3+} to Eu^{3+} ions in the phosphors can simultaneously occur under approximately 290 nm excitation wavelength. However, the energy transfer was effectively observed rather than the individual transitions because the integrated emission intensity of Eu^{3+} transition was enhanced by approximately 91% from $La_{0.95}Eu_{0.05}O_{0.65}F_{1.7}$ to $La_{0.94}Bi_{0.05}O_{0.65}F_{1.7}$ phosphors (Figure S1). The blue-green emission of the $La_{1-p}Bi_pO_{0.65}F_{1.7}$ phosphors centered at 497 nm reached a maximum intensity for a Bi^{3+} content ($p = 0.01$), as shown in Figure 3a. After increasing the Bi^{3+} content, concentration quenching of the relative emission intensity was observed. The increase in the Bi^{3+} content of the phosphors enhanced energy transfer up to some critical value, whereas after this value was reached subsequent increase of Bi^{3+} levels decreased the emission intensity by reducing the critical distance between the Bi^{3+} ions. This resulted in non-radiative energy transfer between Bi^{3+} ions from the electric multipole interactions. The critical distance (R_c) is expressed by the following formula:

$$R_c = 2[3V/4\pi m_c N]^{1/3} \tag{1}$$

where V is the volume of the $La_{0.99}Bi_{0.01}O_{0.65}F_{1.7}$ unit cell, N is the number of available La^{3+} sites for the dopant in the unit cell, m_c is the critical concentration of Bi^{3+}, and R_c is the critical distance for energy transfer [10,22–24,32]. When N and V are 1 and 97.75 $Å^3$, respectively, for $La_{0.99}Bi_{0.01}O_{0.65}F_{1.7}$, R_c ($m_c = 0.01$) is 26.53 Å. The energy transfer mechanism designated an electric multipole interaction because the critical distance is greater than 5 Å. Figure 4a shows the emission spectra of $La_{0.99-q}Bi_{0.01}Eu_qO_{0.65}F_{1.7}$ ($q = 0–0.1$) phosphors under 286 nm excitation. Co-doping of Eu^{3+} into the Bi^{3+}-doped $LaO_{0.65}F_{1.7}$ host structure allowed effective energy transfer from Bi^{3+} to Eu^{3+} under excitation at 286 nm. The energy transfer from Bi^{3+} to Eu^{3+} acted as a sensitizer and an activator, respectively, in the $La_{0.99-q}Bi_{0.01}Eu_qO_{0.65}F_{1.7}$ ($q = 0–0.1$) phosphors, which was activated through the absorption from Bi^{3+} transitions. The energy transfer efficiency (η_T) was evaluated using the following formula:

$$\eta_T = 1 - I_S/I_{SO} \tag{2}$$

where I_S and I_{SO} are the luminescence intensities of the Bi^{3+} sensitizer in the presence and absence of a Eu^{3+} activator, respectively [10,22–24,32]. The emission of Eu^{3+} transitions was maximized when

the Eu^{3+} content in the $La_{0.99-q}Bi_{0.01}Eu_qO_{0.65}F_{1.7}$ ($q = 0$–0.1) phosphors was $q = 0.05$. The energy transfer mechanism could be represented by linear plots of I_{SO}/I_S versus $C_{Bi\text{-}Eu}{}^{\alpha/3}$, where $C_{Bi\text{-}Eu}$ is the concentration of Bi^{3+} and Eu^{3+} ions, with $\alpha = 6$, 8, or 10, corresponding to dipole–dipole, dipole–quadrupole, and quadrupole–quadrupole interactions, respectively, in accordance with Dexter theory [10,22–24,32]. In Figure 4b, when $\alpha = 6$, 8, and 10, the linear plots showed energy transfer from the Bi^{3+} to Eu^{3+} ions with $R^2 = 0.9635$, 0.9894, and 0.9982 in the $La_{0.94}Bi_{0.01}Eu_{0.05}O_{0.65}F_{1.7}$ phosphors, respectively. As the value of α is 10, a closer linear plot is determined for the phosphor, the quadrupole–quadrupole interaction was involved in the energy transfer mechanism of the $La_{0.94}Bi_{0.01}Eu_{0.05}O_{0.65}F_{1.7}$ phosphors. The efficiency of the energy transfer from Bi^{3+} to Eu^{3+} in $La_{0.94}Bi_{0.01}Eu_{0.05}O_{0.65}F_{1.7}$ (EX = 286 nm) phosphors is shown in Figure 4c. The efficiency was gradually enhanced from 23% to 97% as the Eu^{3+} content in the phosphors increased from $q = 0.01$ to 0.1.
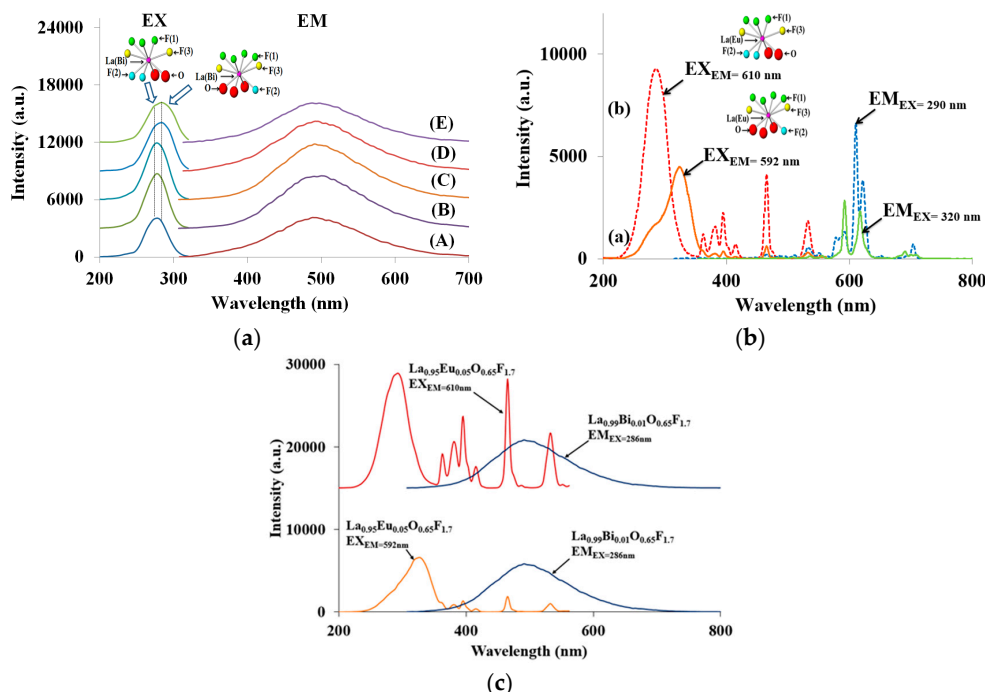
Figure 3. PL excitation and emission spectra of (**a**) $La_{1-p}Bi_pO_{0.65}F_{1.7}$ phosphors (A) $p = 0.001$, (B) 0.005, (C) 0.01, (D) 0.025, and (E) 0.05; and (**b**) $La_{0.95}Eu_{0.05}O_{0.65}F_{1.7}$ phosphors; and (**c**) the excitation spectra of the $La_{0.95}Eu_{0.05}O_{0.65}F_{1.7}$ and the emission spectrum of $La_{0.99}Bi_{0.01}O_{0.65}F_{1.7}$.

Figure 4. *Cont.*

(**c**)
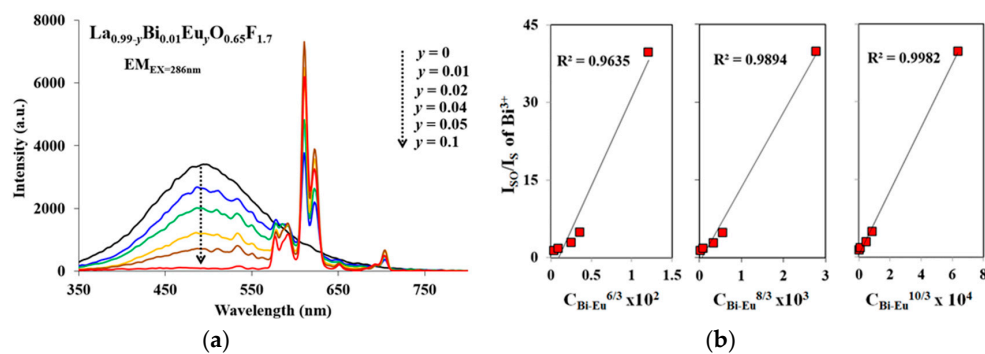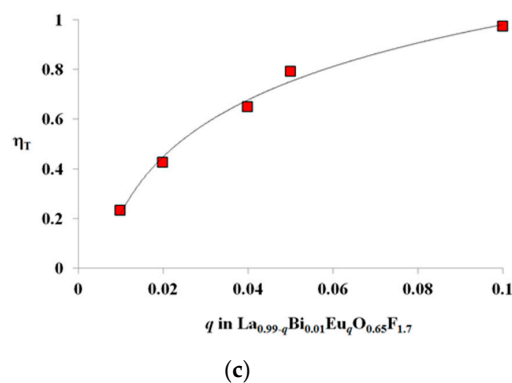
Figure 4. (**a**) The emission spectra of $La_{0.99-q}Bi_{0.01}Eu_qO_{0.65}F_{1.7}$ (q = 0–0.1) phosphors under 286 nm excitation, (**b**) the plot of I_{SO}/I_S versus $C_{Bi-Eu}{}^{\alpha/3}$ (α = 6, 8, 10), and (**c**) energy transfer efficiency from Bi^{3+} to Eu^{3+} in the phosphors.

As shown in Figure 5a, the chromaticity coordinates, x and y, are in accordance with the desired CIE (Commission Internationale de l'Eclairage) values from the blue-green to white and red wavelength regions for $La_{0.99-q}Bi_{0.01}Eu_qO_{0.65}F_{1.7}$ (q = 0–0.1) phosphors (*EX* = 286 nm). The CIE values are summarized in the inset of Figure 5a, along with the values obtained for the phosphors. The CIE coordinates near the blue-green, white, orange, and red regions of the CIE diagram from the phosphors were observed to be x = 0.240 and y = 0.334, x = 0.328 and y = 0.348, x = 0.466 and y = 0.354, and x = 0.591 and y = 0.353, for values of q = 0, 0.02, 0.05, and 0.1, respectively. When the concentration of Eu^{3+} ions in the $La_{0.99-q}Bi_{0.01}Eu_qO_{0.65}F_{1.7}$ phosphors increased from q = 0 to 0.02 and 0.1, the emission colors exhibited a significant shift from blue-green to white, and red emission regions, respectively. These tunable emission lights are appropriate for a high color-rendering index to apply phosphor converted UV-LEDs. This indicates that there was effective energy transfer from Bi^{3+} to Eu^{3+} in the $La_{0.99-q}Bi_{0.01}Eu_qO_{0.65}F_{1.7}$ phosphors. Emission of the $La_{0.99-q}Bi_{0.01}Eu_qO_{0.65}F_{1.7}$ (q = 0–0.1) phosphors under 254, 312, and 365 nm hand-lamp excitation was exhibited blue-green, white, orange, and red colors, as shown in Figure 5b.

(**a**)

(**b**)
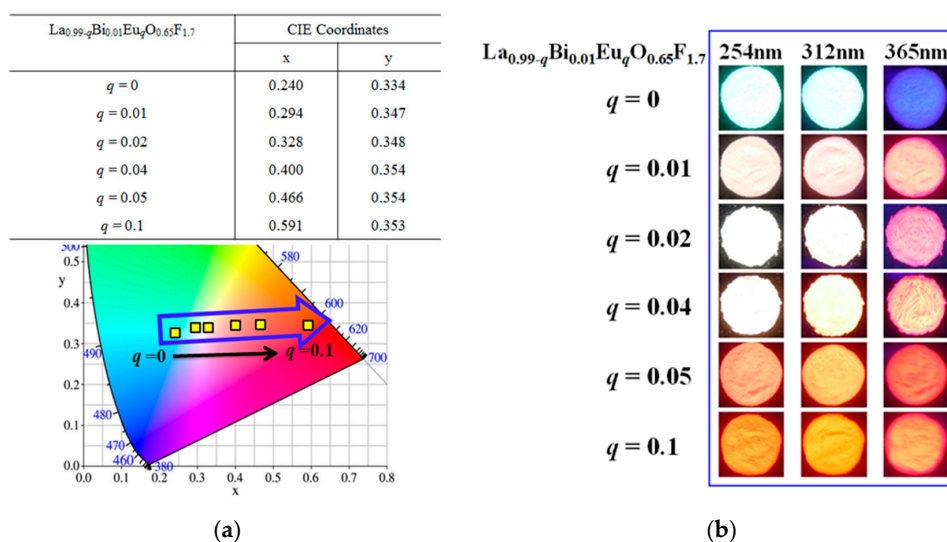
Figure 5. (**a**) The chromaticity coordinates with the desired CIE values of $La_{0.99-q}Bi_{0.01}Eu_qO_{0.65}F_{1.7}$ (q = 0–0.1) phosphors (*EX* = 286 nm) and (**b**) photographs of the emission light from blue-green to white, orange, and red colors in the $La_{0.99-q}Bi_{0.01}Eu_qO_{0.65}F_{1.7}$ phosphors under 254, 312, and 365 nm hand-lamps.

4. Conclusions

Non-stoichiometric tetragonal $La_{1-p-q}Bi_pEu_qO_{0.65}F_{1.7}$ ($p = 0.001–0.05$, $q = 0–0.1$) phosphors were prepared via a solid-state method using a heat treatment at 1050 °C for two hours using NH_4F flux. The site dependency of the Bi^{3+} and Eu^{3+} ions in the $LaF(1)_3F(2)_2O_2F(3)_2$ and $LaF(1)_4F(2)O_3F(3)_2$ polyhedrons of the host structure was analyzed using the PL spectra of the phosphors. The maximum luminescence intensity of the blue-green $La_{1-p}Bi_pO_{0.65}F_{1.7}$ phosphors was obtained when $p = 0.01$. The critical distance (Rc) value for the $La_{0.99}Bi_{0.01}O_{0.65}F_{1.7}$ phosphor was determined to be 26.53 Å. As the Eu^{3+} concentration was increased in $La_{0.99-q}Bi_{0.01}Eu_qO_{0.65}F_{1.7}$ ($q = 0–0.1$) phosphors under 286 nm excitation, an efficient energy transfer from Bi^{3+} to Eu^{3+} occurred, involving quadrupole–quadrupole interactions in the phosphors. The CIE coordinate values attributed to the emissions from blue-green, white, and red for $La_{0.99-q}Bi_{0.01}Eu_qO_{0.65}F_{1.7}$ ($q = 0–0.1$) phosphors were successfully obtained.

References

1. Ye, S.; Xiao, F.; Pan, Y.; Ma, Y.; Zhang, Q. Phosphors in phosphor-converted white light-emitting diodes: Recent advances in materials, techniques and properties. *Mater. Sci. Eng. R Rep.* **2010**, *71*, 1–34. [CrossRef]

2. Schubert, E.F.; Kim, J.K. Solid-State Light Sources Getting Smart. *Science* **2005**, *308*, 1274–1278. [CrossRef] [PubMed]

3. Ahn, Y.N.; Kim, K.D.; Anoop, G.; Kim, G.S.; Yoo, J.S. Design of highly efficient phosphor converted white light-emitting diodes with color rendering indices (R1–R15) ≥ 95 for artificial lighting. *Sci. Rep.* **2019**, *9*, 16848. [CrossRef] [PubMed]

4. Yuan, Y.; Wang, D.; Zhou, B.; Feng, S.; Sun, M.; Zhang, S.; Gao, W.; Bi, Y.; Qin, H. High luminous fluorescence generation using Ce:YAG transparent ceramic excited by blue laser diode. *Opt. Mater. Express* **2018**, *8*, 2760–2767. [CrossRef]

5. Wen, B.; Zhang, D.-F.; Zhang, N.; Feng, J.-K.; Jiang, B.; Pan, F.-S.; Zhang, Y.; Yang, L. Effect of grain size on the luminescent properties of Ce^{3+} doped $Y_3Al_5O_{12}$ ceramic phosphor plates. *Ceram. Int.* **2020**, *46*, 10452–10456. [CrossRef]

6. Zhang, S.; Hao, Z.; Zhang, L.; Pan, G.-H.; Wu, H.; Wu, H.; Luo, Y.; Liu, X.; Zhangb, H.; Zhang, J. Observation of a red Ce^{3+} center in $SrLu_2O_4$:Ce^{3+} phosphor and its potential application in temperature sensing. *Dalton Trans.* **2019**, *48*, 5263–5270. [CrossRef]

7. Wan, J.; Liu, Q.; Liu, G.; Zhou, Z.; Xie, R.-J. $Y_2Si_4N_6C$:Ce^{3+} carbidonitride green-yellow phosphors: Novel synthesis, photoluminescence properties, and applications. *J. Mater. Chem. C* **2017**, *5*, 6061–6070. [CrossRef]

8. Xie, M. Structure, site occupancies, and luminescence properties of $Ca_{10}M(PO_4)_7$: Ce^{3+} (M = Li, Na, K) phosphors. *J. Alloys Compd.* **2019**, *775*, 1129–1135. [CrossRef]

9. Yang, S.; Park, S. Ca^{2+}-substitution effects in $Ba_{9-x}Ca_xAl_2Si_6O_{24}$:$Ce^{3+}$, Na^+ phosphors. *Opt. Mater.* **2020**, *99*, 109548. [CrossRef]

10. Zou, Y.; Min, X.; Liu, Z.; Yu, L.; Liu, B. Photoluminescent properties and energy transfer mechanism of Tb^{3+}-Ce^{3+} doped $CaSi_2O_2N_2$ oxynitride phosphors. *Mater. Res. Bull.* **2020**, *124*, 110769. [CrossRef]

11. Yang, S.; Park, S. Promising green $Sr_5B_3O_9F$: Ce^{3+}/Tb^{3+}/Na^+ phosphors for NUV executable LED applications. *J. Alloys Compd.* **2020**, *834*, 155094. [CrossRef]

12. Yang, W.; Park, S. Predominant green emission of Ce^{3+}–Tb^{3+} activated $Y_7O_6F_9$ phosphors. *RSC Adv.* **2016**, *6*, 12652–12656. [CrossRef]

13. Xia, Z.; Liu, R.-S. Tunable Blue-Green Color Emission and Energy Transfer of $Ca_2Al_3O_6F$:Ce^{3+},Tb^{3+} Phosphors for Near-UV White LEDs. *J. Phys. Chem. C* **2012**, *116*, 15604–15609. [CrossRef]

14. Fu, X.; Fang, L.; Niu, S.; Zhang, H. Luminescence properties and energy transfer investigations of $SrMgSi_2O_6$:Ce,Tb phosphors. *J. Lumin.* **2013**, *142*, 163–166. [CrossRef]

15. Song, K.; Zhang, J.; Liu, Y.; Zhang, C.; Jiang, J.; Jiang, H.; Qin, H.-B. Red-Emitting Phosphor $Ba_9Lu_2Si_6O_{24}$:Ce^{3+},Mn^{2+} with Enhanced Energy Transfer via Self-Charge Compensation. *J. Phys. Chem. C* **2015**, *119*, 24558–24563. [CrossRef]

16. Xu, Z.; Xia, Z.; Lei, B.; Liu, Q. Full color control and white emission from CaZnOS:Ce^{3+},Na^+,Mn^{2+} phosphors via energy transfer. *J. Mater. Chem. C* **2016**, *4*, 9711–9716. [CrossRef]

17. Yun, H.; Park, S. Blue-white-orange tunable $Ba_6Ca_3YAlSi_6O_{24}$:Eu^{2+},Mn^{2+} phosphors for NUV-pumped LEDs. *Opt. Mater.* **2018**, *86*, 600–605. [CrossRef]

18. Park, S. Ce^{3+}–Mn^{2+} cooperative $Ba_9Y_2Si_6O_{24}$ orthosilicate phosphors. *Mater. Lett.* **2014**, *135*, 59–62. [CrossRef]

19. Kang, F.; Zhang, Y.; Peng, M. Controlling the Energy Transfer via Multi Luminescent Centers to Achieve White Light/Tunable Emissions in a Single-Phased X2-Type Y_2SiO_5:Eu^{3+},Bi^{3+} Phosphor For Ultraviolet Converted LEDs. *Inorg. Chem.* **2015**, *54*, 1462–1473. [CrossRef]

20. Wang, L.; Sun, Q.; Liu, Q.; Shi, J. Investigation and application of quantitative relationship between sp energy levels of Bi^{3+} ion and host lattice. *J. Solid State Chem.* **2012**, *191*, 142–146. [CrossRef]

21. Chen, L.; Zheng, H.; Cheng, J.; Song, P.; Yang, G.; Zhang, G.; Wu, C. Site-selective luminescence of Bi^{3+} in the YBO_3 host under vacuum ultraviolet excitation at low temperature. *J. Lumin.* **2008**, *128*, 2027–2030. [CrossRef]

22. Li, K.; Fan, J.; Shang, M.; Lian, H.; Lin, J. $Sr_2Y_8(SiO_4)_6O_2$:Bi^{3+}/Eu^{3+}: A single-component white-emitting phosphor via energy transfer for UV w-LEDs. *J. Mater. Chem. C* **2015**, *3*, 9989–9998. [CrossRef]

23. Yang, S.; Kim, H.; Park, S. Color-tunable luminescence in $Y_{7(1-m-n-z)}Bi_{7m}Dy_{7n}Eu_{7z}O_6F_9$ (m = 0.001–0.05, n = 0–0.1, z = 0.005, 0.01) phosphors. *Opt. Mater.* **2018**, *77*, 154–160. [CrossRef]

24. Yun, H.; Kim, S.-H.; Park, S. Bi^{3+}, Eu^{3+}-doped $Ba_9Y_2Si_6O_{24}$ phosphors based on the site-selected substitution. *Opt. Mater.* **2017**, *72*, 571–577. [CrossRef]

25. Yadav, R.; Rai, S. Surface analysis and enhanced photoluminescence via Bi^{3+} doping in a Tb^{3+} doped Y_2O_3 nano-phosphor under UV excitation. *J. Alloys Compd.* **2017**, *700*, 228–237. [CrossRef]

26. Park, J.Y.; Jung, H.C.; Lee, H.; Moon, B.K.; Jeong, J.H.; Son, S.-M.; Kim, J.-H. Enhanced green emission from Tb^{3+}–Bi^{3+} co-doped $GdAlO_3$ nanophosphors. *Mater. Res. Bull.* **2010**, *45*, 572–575. [CrossRef]

27. Noh, W.; Park, S. Synthesis and distinct up-converting behaviors of Er^{3+}, Yb^{3+} doped LaOF and $LaO_{0.65}F_{1.7}$ phosphors. *Opt. Mater.* **2017**, *66*, 589–594. [CrossRef]

28. Hölsä, J.; Folkesson, B.; Thiem, J.; Kofod, P.; Elding, L.I.; Trabjerg, I. Effect of Non-stoichiometry on the Luminescence Properties of Lanthanum Oxyfluorides. *Acta Chem. Scand.* **1991**, *45*, 583–587. [CrossRef]

29. Park, S. Distinct structural and optical correlations of $Y_{1-x}Eu_xOF$ and $Y_{n(1-x)}Eu_{nx}O_{n-1}F_{n+2}$ (x = 0.001–0.1, n = 6, 7) vernier phosphors. *J. Lumin.* **2015**, *166*, 176–179. [CrossRef]

30. Yen, W.M.; Shionoya, S. *Phosphor Handbook*; CRC Press: Boca Raton, FL, USA, 1999.

31. Huang, C.-H.; Chen, T.-M.; Liu, W.-R.; Chiu, Y.-C.; Yeh, Y.-T.; Jang, S.-M. A Single-Phased Emission-Tunable Phosphor $Ca_9Y(PO_4)_7$:Eu^{2+},Mn^{2+} with Efficient Energy Transfer for White-Light-Emitting Diodes. *ACS Appl. Mater. Interfaces* **2010**, *2*, 259–264. [CrossRef]

32. Xia, M.; Zhao, W.; Zhong, J.; Shi, P.; Liao, Z.; Liu, X.; Song, J.; Luo, L.; Ma, L.; Nie, Z. Tunable luminescence of blue-green emitting $NaBaBO_3$:Ce^{3+},Tb^{3+} phosphors for near-UV light emitting diodes. *J. Lumin.* **2020**, *220*, 116957. [CrossRef]